Investigation of the Ligand Exchange Behavior of Square-Planar Nickel(II) Complexes by X-ray Absorption Spectroscopy and X-ray Diffraction

Martin P. Feth,*[a] Axel Klein,*[b] and Helmut Bertagnolli[a]

Keywords: Nickel / Ligand exchange / EXAFS spectroscopy / XANES / X-ray diffraction

The local structure of nickel and bromine in three square-planar nickel(II) complexes [(2,2′-bipyridyl)(bromo)(mesityl)-nickel(II)] (**1**), [(bromo)(*N*,*N*-diisopropyl-1,2-ethanediimine)-(mesityl)nickel(II)] (**2**), [(bromo)(mesityl)bis(triphenylphosphane)nickel(II) (**3**)] and their ligand exchange behavior towards several solvents has been determined by means of X-ray Absorption Near Edge Spectroscopy (XANES), Extended X-ray Absorption Fine Structure Spectroscopy (EXAFS), X-ray Diffraction (XRD), multinuclear NMR and UV/Vis spectroscopy. Several square-planar and octahedral nickel(II) complexes were prepared and spectroscopically characterized as reference compounds. The exchange behavior strongly depends on the nature of the incoming donor ligand (solvent molecule). In some cases the substitution of one or more ligands was accompanied by conservation of the square-planar geometry. In other solvents the geometry changed from square-planar to octahedral. The structural information obtained is important to the further development of such nickel(II) complexes as catalysts for various applications.

Introduction

Organonickel(II) complexes are widely used in organometallic catalysis. One of the first benchmarks was the (phosphane)nickel complexes used in the Shell Higher Olefin Process (SHOP)[1−7] (Scheme 1).

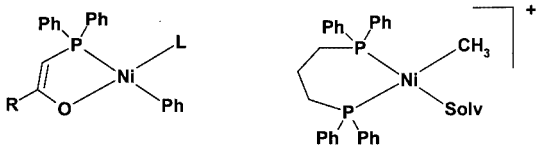

Scheme 1. Nickel catalysts for the oligomerization of olefins in the Shell Higher Olefin Process (SHOP) (**A**)[2−5] (left) or for copolymerization of ethene with CO (**B**)[6,7] (right)

A crucial requirement for these two systems to act as catalysts is that they contain a labile ligand (L or Solv) − as exhibited by the highly reactive catalysts for olefin polymerization developed over the last decade, mainly by Brookhart [1,2,8−14]. The active catalyst species are prepared from dialkylnickel precursor complexes as shown in Scheme 2.

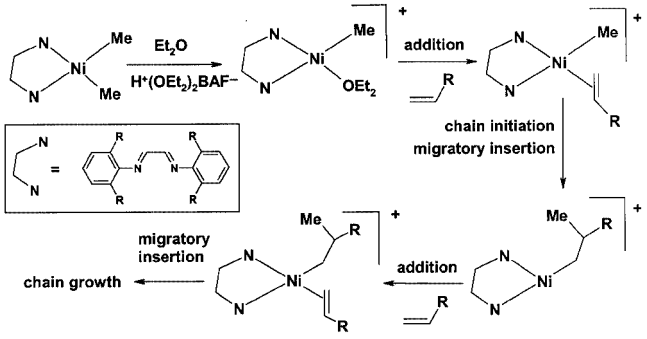

Scheme 2. (α-Diimine)nickel complexes (diimine = 1,4-diazabutadiene) as catalysts for the polymerization of olefins;[2] preparation of the active catalyst species (top) and elemental steps in polymerization catalysis (bottom); BAF = perfluorinated tetraarylborates

Recently, we have investigated organonickel complexes of the type [(diimine)Ni(R)X] (R = alkyl or aryl; X = Cl or Br) to develop an alternative route to catalytically active species. We originally intended to abstract X by the addition of silver salts or related reagents; however, in polar solvents the complexes already showed a considerable degree of dissociation into the ionic species $[(diimine)Ni(R)(Solv)]^+$ and X^-, depending on X, the polarity of the solvent and the bulkiness of the R group [2,8,9,11−13]. With X = Cl the complexes are more inert towards X-dissociation but are very sensitive to hydrolysis. Complexes with X = Br are much more reactive towards dissociation but are quite inert towards water. Alkyl derivatives (R = alkyl) are very reactive to both dissociation and water whereas aryl complexes are relatively stable.[15,16] Dissociation can be enormously accel-

[a] Institut für Physikalische Chemie, Universität Stuttgart, Pfaffenwaldring 55, 70550 Stuttgart
Fax: (internat.) + 49-711/685-4443
E-mail: m.feth@ipc.uni-stuttgart.de
[b] Institut für Anorganische Chemie, Universität Stuttgart, Pfaffenwaldring 55, 70550 Stuttgart
Fax: (internat.) + 49-711/685-4165
E-mail: aklein@iac.uni-stuttgart.de
Supporting information for this article is available on the WWW under http://www.eurjic.org or from the author.

erated by electrochemical reduction of the starting complexes. The rapid loss of Br^- after reduction to the radical anionic species $[(diimine)Ni(R)Br]^{\cdot -}$ can only be slowed to a measurable rate for the very bulky mesityl group and at quite low temperatures.[17−20] The dissociation reactions yield species which should be quite reactive in the catalytic polymerization of olefins. However, we first wanted to examine in detail the structural aspects of these ligand exchange reactions (X^- to Solv) and to determine whether, in these media, further ligand exchange reactions occur that would lead to the replacement of the diimine ligand. To our astonishment this question has never been investigated thoroughly in mechanistic studies of olefin polymerization or related reactions.[1,6,7,9,11,21] In the nonpolar media used for the reactions and the applied excesses of ligand there is no need to consider ligand loss. However, if the reactions are to be extended to highly polar solvents with donor capabilities, or the ligand appears to be the "cost-determining step" and should not be used in excess, the partial or total loss of the chelate ligand (here the diimine) has to be considered, since it might influence the catalytic mechanism. We therefore investigated the ligand exchange reactions of the complexes [(diimine)Ni(Mes)Br] and also *trans*-$[(PPh_3)_2Ni(Mes)Br]$. The latter is not only the starting complex for the preparation of the *cis*-configured diimine complexes but shows the same dissociation lability and has been the subject of a related kinetic study.[22] Also it was previously used to catalyze the co-dimerization of butadiene and ethylene.[23] The combination of the bulky R group and the good leaving group Br^- renders these systems very suitable for a detailed mechanistic study since the timescale of the reactions lie in the range of minutes to hours. From the available diimine complexes we have chosen two different types: 2,2′-bipyridine (bpy), a classical aromatic diimine ligand, and *N*,*N*-diisopropyl-1,4-diazabutadiene (*i*Pr-DAB), a "Brookhart"-type ligand (see Scheme 2) developed some five decades ago.[24−27] in addition to the standard spectroscopic techniques (multinuclear NMR or UV/Vis absorption spectroscopy) we have made great use of EXAFS spectroscopy to investigate the ligand exchange reactions. For studies were crystalline samples are not available or of isotropic (X-ray amorphous) media like solutions, or powders, EXAFS is a powerful tool to elucidate the coordination sphere of such catalytically relevant species.[28−31] We used EXAFS spectroscopy at the nickel *K*-edge as well as on the bromine *K*-edge to investigate ligand exchange reactions in these complexes in solution as well as on separately prepared and isolated samples of possible intermediates. Molecular structures determined by XRD from single crystals helped to adjust reasonable fitting models. Investigation of the XANES region of an X-ray absorption spectra is also a powerful tool for the determination of the geometry of the first coordination shell and the oxidation state of an absorbing atom.[32,33] Emphasis can be given to the so-called pre-edge peaks (short: pre-peaks), which are related to electric dipole transitions from inner shells to unfilled bound states, e.g. 1s → 3d. These pre-peaks are very sensitive to geometrical changes in the first coordination shell of the absorbing atom. The symmetry of the first shell determines if certain pre-peaks appear in the spectrum or are symmetrically forbidden. For the square-planar Ni^{II} complexes the XANES investigations focus on the pre-peaks assigned to the 1s → 3d and 1s → $4p_z$ transitions.[34,35]

Results and Discussion

UV/Vis Absorption and Multinuclear NMR Spectroscopy in Solution

The bright colors of the compounds under investigation can be used to monitor their reactions. The complexes [(diimine)Ni(Mes)Br] show characteristic solvatochromic absorptions in the visible region[18,21,36,37] and dissolving them in non- to moderately coordinating solvents, such as toluene, CH_2Cl_2, THF, acetone, propylene carbonate (PC) and *N*,*N*-dimethylformamide (DMF), leads only to the expected solvatochromic shift. Solutions with pyridine or acetonitrile as solvent, however, show markedly blue-shifted absorption maxima within a few seconds {as shown for [(bpy)Ni(Mes)Br] in Figure 1}. These rapid reactions are followed by slower ones and the observed absorption bands were again shifted to higher energies. For the reaction of [(bpy)Ni(Mes)Br] in MeCN the rate of the first reaction was determined as $k = 0.324(6)\ M^{-1}\ s^{-1}$, assuming a first-order mechanism. We assign this to the dissociation of the bromide ligand and substitution by MeCN. The second reaction is much slower [$k = 0.0041(3)\ M^{-1}\ s^{-1}$] and is assigned to the replacement of the chelate ligand. This is deduced from the corresponding reaction in pyridine solution, where the rate constant is comparable [$k = 0.0029(3)\ M^{-1}\ s^{-1}$] and the resulting absorptions are coincident with those of the pyridine complex $[(py)_3NiMes]^+$ (see Exp. Sect.).

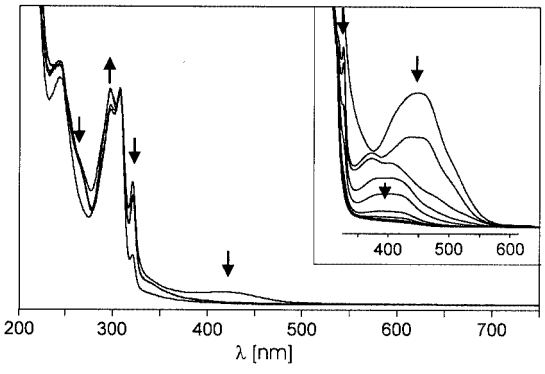

Figure 1. UV/Vis absorption spectra of [(bpy)Ni(Mes)Br] in acetonitrile (MeCN), immediately after dissolution and 3, 4.5 and 21 h later; insert: 20 s, 60 s, 180 s, 360 s, 540 s, and 720 s after dissolution

^1H NMR spectroscopy gives no sign of (partial) dissociation of the chelate ligand in the first minutes after dissolving, thus supporting the assumed reaction sequence. Subsequently, several reaction products appear that cannot be assigned unambiguously. After a prolonged reaction (several days) only in the case of pyridine we could clearly identify $[(py)_3Ni(Mes)]^+$ and the free ligand. In MeCN

numerous soluble products are found, along with insoluble green material.

The complex $[(PPh_3)_2Ni(Mes)Br]$ exhibits, in solvents such as toluene, CH_2Cl_2 or acetone, a solvent-invariant, weak long-wavelength absorption band with a maximum around 450 nm.[22] In pyridine solution a reaction occurs that can be monitored by a decrease of this band and the appearance of the blue-shifted maximum at around 410 nm. After this relatively fast reaction [$k(1) = 0.284(9)$ м$^{-1}$ s^{-1}], a second slower reaction follows with $k(2) = 0.0061(5)$ м$^{-1}$ s^{-1}. The reactions were confirmed by ^{1}H and ^{31}P NMR spectroscopy as identical to those of the diimine complexes.[11]. The ^{31}P NMR signal at $\delta = 20.2$ ppm for the starting complex is replaced by a singlet at $\delta = 27$ ppm that can be assigned to *trans*-$[(PPh_3)_2Ni(Mes)(py)]^+$ (see Exp. Sect.). Finally, after 36 h, only free PPh_3 ($\delta = -5$ ppm) is detected in solution. The ^{1}H NMR spectrum confirms the formation of $[(py)_3Ni(Mes)]^+$. In THF solution the reaction seems to stop after the first sequence and the resulting ^{31}P signal at $\delta = 29$ ppm is assigned to the solvent-coordinated species $[(PPh_3)_2Ni(Mes)(THF)]^+$. For a ligand-exchange reaction using thiocyanate (SCN^-) Martinez and Muller derived a two-term rate law, with $k_s = 5.2 \pm 0.6 \times 10^{-2}$ mol^{-1} s^{-1}, for the exchange of bromide versus the acetone solvent and $k_{an} = 3.0 \pm 0.4 \times 10^{-1}$ mol^{-1} s^{-1} for the subsequent replacement of acetone by SCN^-. On varying R in $[(PPh_3)_2Ni(R)Br]$ from C_6H_4Cl to C_6Cl_5 the k_{an} value lies in the range 43 to 6.6×10^{-4} with mesityl occupying an intermediate position.[22] Our experiments (see also EXAFS) confirm that even weakly coordinating solvents such as acetone or THF can replace bromide to form $[(PPh_3)_2Ni(Mes)(Solv)]^+$, which is in sharp contrast to the behavior of [(bpy)Ni(Mes)Br]. This is due to the strong *trans* effect of the mesityl ligand. Since our substitution reactions on $[(PPh_3)_2Ni(Mes)Br]$ were performed in neat pyridine or other media that are potential ligands, we fitted our kinetic data according to a first-order rate law, thus deviating from the established two-term rate law.[22] Our $k(1)$ value agrees excellently with the k_{an} measured by Martinez and Muller, indicating that SCN^- and pyridine are of comparable σ-donor capability. In acetonitrile the first rapid reaction leads to a green solution. Inspection of the absorption spectrum shows weak long-wavelength absorptions at 1228 nm (8143 cm^{-1}; $\varepsilon = 40$ м$^{-1}$·cm^{-1}) and 630 nm (15873 cm^{-1}; $\varepsilon = 160$ м$^{-1}$·cm^{-1}; with a shoulder at 681 nm). The latter is responsible for the observed green color. In the UV region, shoulders at 431 nm (23202 cm^{-1}) and 419 nm (23877 cm^{-1}) are discernible and the spectrum is dominated by an intense band at 267 nm (37450 cm^{-1}; $\varepsilon = 23000$ м$^{-1}$cm^{-1}). The long-wavelength bands are quite weak and typical for ligand field transitions of nickel(II) complexes.[38,39] We assume a tetrahedral coordination of the ligands in $[(PPh_3)_2Ni(Mes)(MeCN)]^+$, the product of the first substitution reaction. An octahedral coordination was excluded because of the bulkiness of the Mes and PPh_3 ligands. The corresponding absorptions were assigned to $\nu_1 = {}^3T_2(F) \rightarrow {}^3T_1(F)$; $\nu_2 = {}^3A_2(F) \rightarrow {}^3T_1(F)$ and $\nu_3 = {}^3T_1(P) \rightarrow {}^3T_1(F)$. Such transitions are usually more intense than those of octahedral species and exhibit splitting due to spin-orbit coupling. The ^{31}P NMR spectra of such green solutions show the presence of a singlet at $\delta = 21.7$ ppm. In addition, two further singlets at $\delta = 20.3$ ppm (starting complex) and $\delta = 19.3$ ppm (1/20 intensity of the $\delta = 21.7$ ppm signal) are observed whereas free PPh_3 is not found. The ^{1}H NMR spectra confirm the presence of several species, but line broadening precludes further assignments.. Apart from different degrees of substitution, an equilibrium between tetrahedral and square-planar conformations of an individual species might account for the complicated behavior, as has been described for $[(PEtPh_2)_2NiBr_2]$.[40,41] As tetrahedral nickel(II) species should be paramagnetic ($S = 1$), which might explain the poor NMR spectroscopic data, an ESR investigation of these species is planned.

Structural Studies on the [(bpy)Ni(Mes)Br] System

Crystal Structure

The crystal structure of [(bpy)Ni(Mes)Br]·THF (Figure 2) shows two very similar, but independent, molecules in the unit cell. Both structures exhibit the expected square-planar environment of the nickel atoms, with only slight tetrahedral distortions [N(11)−Ni(1)−N(12) towards C(11)−Ni(1)−Br(1) of 8.6° or 12.1°, respectively].

The bond lengths of **1** and **2** are very similar and lie in the expected range.[17,42,43] However, while the interplanar angle between the two pyridine moieties is negligible for **1** (1.9°) it is appreciable for **2** (10.5°). A further distortion for **2** concerns the C(21)−Ni(2)−N(22) angle of 170.4(3), which deviates markedly from the idealized 180°. For **1** we found 176.2(3)°. Both molecules are similar to the recently described dimesityl complex $[(bpy)Ni(Mes)_2]$.[17] The distortion of the coordination plane in $[(bpy)Ni(Mes)_2]$ is very much like that in **2** (12.4°) whereas the pyridine interplanar angle (3.2°) is close to that of **1**. Many other molecular parameters are very similar for these three structures, with the notable exception of the Ni−N distance *trans* to the Br ligand, which is markedly shorter than the others in agreement with the expected *trans* influence.

XANES Investigations

In the XANES spectra of the square-planar Ni^{II} at the Ni *K*-edge complexes two pre-edge peaks can be observed [Figure 3 (a)]. The pre-peak at about 8333 eV can be assigned to a $1s \rightarrow 3d$ electron transition, while the second peak, which occurs at about 8337 eV, is due to a $1s \rightarrow 4p_z$ transition.[34,35] In octahedral Ni^{II} complexes the $1s \rightarrow 3d$ transition as well as the $1s \rightarrow 4p_z$ transition are forbidden; however, the small orbital mixing by lower symmetry gives some probability for the $1s \rightarrow 3d$ transition. Thus, in octahedral complexes the $1s \rightarrow 4p_z$ pre-peak at 8337 eV is absent and the $1s \rightarrow 3d$ pre-peak shows a much smaller intensity than in square-planar complexes [34,35,44]. Therefore octahedral and square-planar complexes can be distinguished by the presence or absence of the $1s \rightarrow 4p_z$ transition.

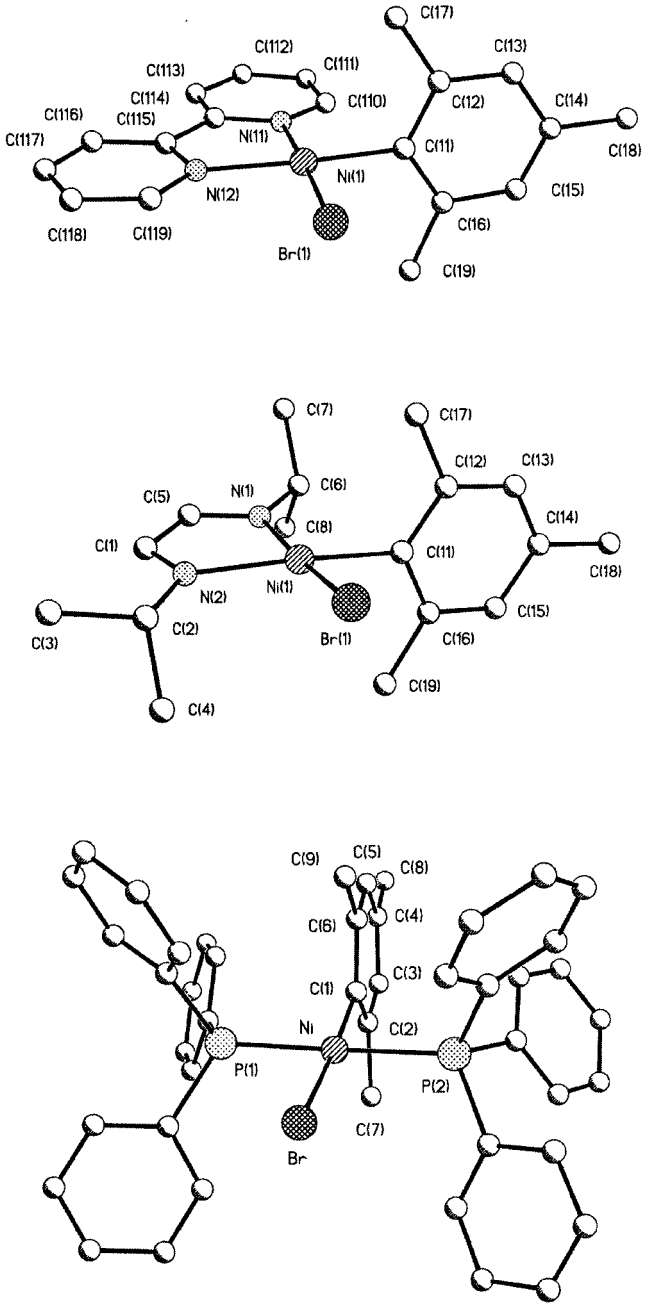

Figure 2. Molecular structure of the investigated Ni^{II} complexes: [(bpy)Ni(Mes)Br] (**1**) (top), [(*i*Pr-DAB)Ni(Mes)Br] (**2**) (center) and $[(PPh_3)_2Ni(Mes)Br]$ (**3**) (bottom)

In Figure 3 (a) the pre-edge and XANES region at the Ni *K*-edge of the solid complex **1** is shown in comparison with its solutions in pyridine and acetonitrile. As an octahedral reference compound the XANES spectra of $[(1,10\text{-phenanthroline})_2NiBr_2]$ is also shown. In the pure, solid square-planar complex (solid line) the typical two pre-peaks for the $1s \rightarrow 3d$ and $1s \rightarrow 4p_z$ transitions are clearly visible. The solution in pyridine (dotted line) also shows these two pre-peaks; thus the local structure around the Ni atoms remains in a square-planar geometry. The XANES spectra of the dissolved complex **1** in THF, collidine, or acetone also reveal retention of the square-planar geometry.

In contrast to the pyridine solution the XANES region of **1** in acetonitrile solution shows only the weak pre-peak of the $1s \rightarrow 3d$ transition, similar to the XANES region of the octahedral reference complex $[(phen)_2NiBr_2]$. This clearly hints that the complex has changed from a square-planar to an octahedral structure. The same behavior was observed for other nitriles (benzonitrile or butyronitrile), in alcohols, e.g. methanol in Figure 3 (b), and a mixture of acetone and water (molar ratio 1:1.23).

Figure 3 (b) the XANES region of [(bpy)Ni(Mes)(OMe)] shows two pre-peaks, indicating a square-planar geometry. This compound was obtained from the reaction of [(bpy)-Ni(Mes)Br] with sodium methoxide in THF (see Exp. Sect.). The same species was observed upon prolonged reaction of [(bpy)Ni(Mes)Br] in methoxide solutions. Retention of the square-planar geometry, even in the presence of a large excess of methoxide, indicates that formation of the octahedral species requires the acid protons of the solvent. Presumably the loss of the shielding mesityl ligand is the crucial step.

Figure 3 (c) shows the XANES spectra of the solid products of [(bpy)Ni(Mes)Br] in several linear primary and secondary alcohols after 16 h reaction. In methanol only the $1s \rightarrow 3d$ transition can be seen; thus, it can be concluded that the Ni^{II} complex has completely changed its geometry from square-planar to octahedral. In other alcohols after the same reaction time, the $1s \rightarrow 4p_z$ transition is still observable, but the signal is significantly weaker than that of the pure complex. This can be explained by a mixture of square-planar and octahedral species in the investigated reaction products. The highest $1s \rightarrow 4p_z$ signal is observed in 2-butanol and the signal decreases in the sequence 2-butanol, 2-propanol, 1-propanol, ethanol and methanol. Thus, the reaction rate decreases with increasing carbon-chain length and is higher in primary alcohols. This is also in agreement with the sequence of the acidity constants of the corresponding alcohols.[45–47]

EXAFS Investigations

The obtained structural parameters of the system [(bpy)-Ni(Mes)Br] system, determined by EXAFS at the Ni *K*- and Br *K*-edge, are summarized in Table 1. Table 2 presents results from the EXAFS fitting procedure of several octahedral and square-planar reference compounds, also measured at the Ni *K*- and Br *K*-edge.

Figure 4 shows the k^3-weighted experimental and Fourier-transformed (FT) EXAFS function of the solid complex **1** in comparison with its solutions in THF and pyridine at the Ni *K*-edge.

The fit of the Ni *K*-edge EXAFS spectrum of the solid complex was performed with three different coordination shells. The first shell at about 1.9 Å consists of the two coordinating nitrogen atoms of the bipyridine ligand and the carbon atom of the mesityl ligand. Because of the similar distances of these backscatterers [XRD: $r(Ni-C_{Mes})$ = 1.896 Å, $r(Ni-N_{bpy,1})$ = 1.896 Å, $r(Ni-N_{bpy,2})$ = 1.984 Å], they cannot be fitted separately and thus were fitted as one

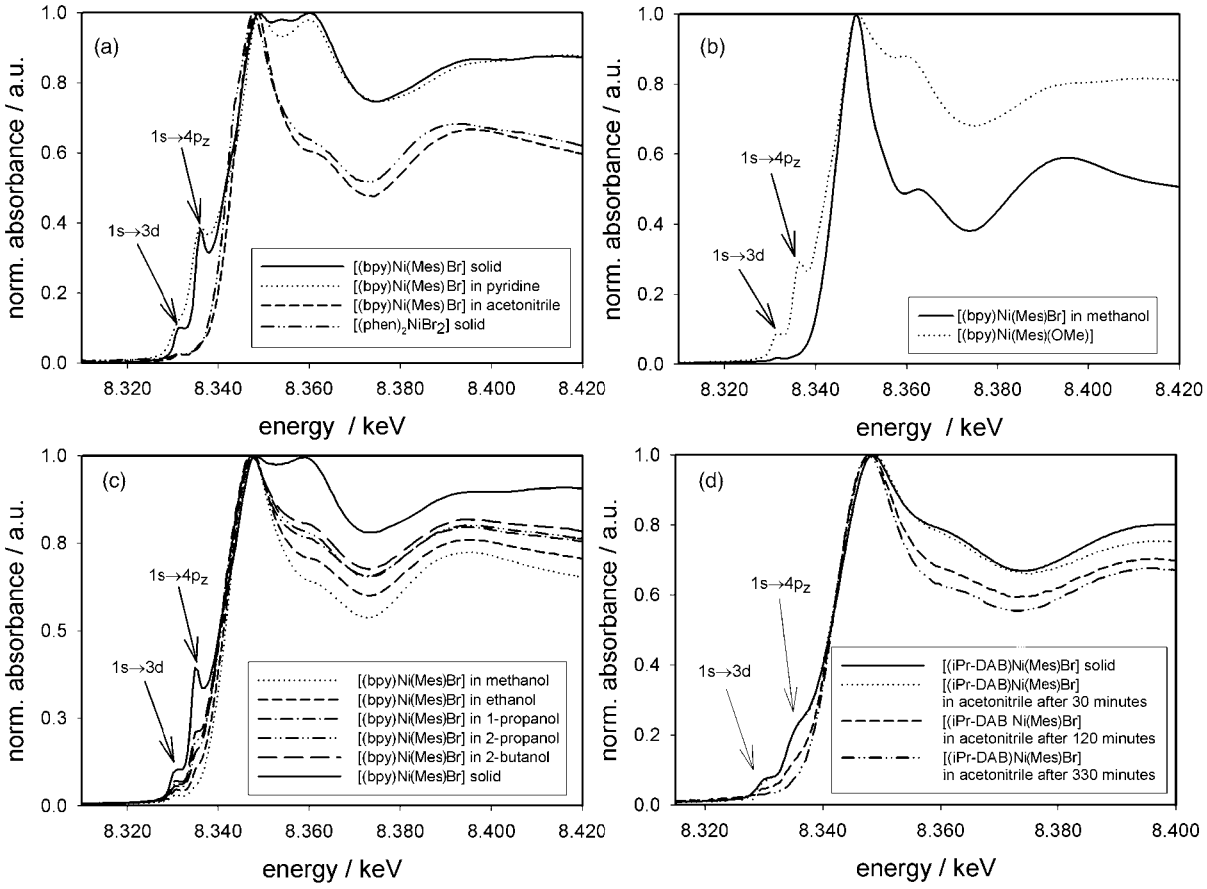

Figure 3. (a) Comparison of the Ni *K*-edge XANES regions of solid [(bpy)Ni(Mes)Br] and its solutions in pyridine and acetonitrile with solid $[(phen)_2NiBr_2]$; (b) comparison of the Ni *K*-edge XANES regions of the solid products of [(bpy)Ni(Mes)Br] in methanol after 48 h reaction with [(bpy)Ni(Mes)Br] + MeONa in THF; (c) comparison of the Ni *K*-edge XANES regions of the solid products of [(bpy)Ni-(Mes)Br] in methanol, ethanol, 1-propanol, 2-propanol and 2-butanol after 16 h reaction; (d) comparison of the Ni *K*-edge XANES regions of solid [(*i*Pr-DAB)Ni(Mes)Br] and its solution in acetonitrile over time

shell with nitrogen amplitude- and phase-functions. The determined distance of 1.92 Å as well as the coordination number of 3.1 is in good agreement with the average value of 1.93 Å known from XRD. The bromine backscatterer was found at 2.30 Å with a coordination number of 1.0. These values are in very good agreement with those found from the Br *K*-edge EXAFS spectrum [N = 0.9, r(Ni−Br) = 2.30 Å] and from the single-crystal XRD experiment (2.30 Å). The third coordination shell was fitted with carbon backscatterers and led to an Ni−C distance of 2.81 Å and a coordination number of 5.6. Possible candidates for these carbon backscatterers are the C(12) and C(16) atom of the mesityl ligand and the C(114), C(115) and C(110) atoms of the bipyridine ligand. This is also in agreement with the relatively high Debye−Waller factor of this shell (σ = 0.110 Å), which is a consequence of the distance distribution of the backscatterers from 2.77 to 2.91 Å. As the observed coordination numbers of the fitted three shells are in good agreement with the expected values, multiple scattering does not seem to play a significant role. Therefore the definition of multiple scattering units is unnecessary.

As can be seen from Figure 4 (a and b), there are only negligible differences between the spectra of the solid complex and its solution in THF. The Ni *K*-edge EXAFS spectra of [(bpy)Ni(Mes)Br] solutions in acetone, THF, or collidine yielded almost identical structural parameters to those found for the solid complex (Table 1). Thus, in these solvents, the complex does not undergo structural changes. This is consistent with observations from the Ni XANES region. In pyridine, however, upon dissolving the initial red complex the solution immediately turned yellow. Fourier-transform of the experimental EXAFS spectrum of the pyridine solution [Figure 4 (b)] shows, in comparison with the solid complex, a higher intensity for the peak at about 1.9 Å and the loss of bromine atom signal at ca. 2.3 Å. Fitting the EXAFS function revealed an increase in the coordination number of the first coordination shell from 3 to 4, with an average distance of 1.88 Å. Bromine backscatterers did not contribute to the EXAFS function. As the XANES region of the pyridine solution shows the typical pre-peaks for a square-planar geometry around the Ni atoms, it can be concluded that the bromine atom has been substituted in an associative process by a pyridine solvent molecule. To determine whether the bipyridine ligand has also been replaced by pyridine, several pyridine derivatives of [(bpy)Ni(Mes)Br] have been synthesized and characterized by EXAFS, and ^{1}H and ^{13}C NMR spectroscopy. The results of the EXAFS experiments on these reference compounds at the Ni *K*- and Br *K*-edge are reported

Table 1. Structural parameters of solid [(bpy)Ni(Mes)Br] and its reaction products in various solvents, determined from Ni *K*- and Br *K*-edge EXAFS spectra [absorber A, backscatterer Bs, A−Bs distance *r*, coordination number *N*, Debye-Waller factor σ with calculated deviation, shift of the energy threshold energy ΔE_0 and the fit-index *R* (AFAC = 0.8)]

	A−Bs	*r* [Å]	N	σ [Å]	ΔE_0 [eV]	*k*-range [Å^{-1}] fit-index
Pure	Ni−C/N	1.92 ± 0.02	3.1 ± 0.3	0.081 ± 0.008	28.0	3.60−14.90
EXAFS in the solid state	Ni−Br	2.30 ± 0.02	1.0 ± 0.2	0.062 ± 0.011		21.8
	Ni−C	2.81 ± 0.03	5.6 ± 1.7	0.110 ± 0.030		
	Br−Ni	2.30 ± 0.02	0.9 ± 0.1	0.060 ± 0.006	14.5	3.60−11.30
						23.5
THF	Ni−C/N	1.90 ± 0.02	2.7 ± 0.3	0.073 ± 0.008	28.2	3.60−13.90
EXAFS in solution	Ni−Br	2.29 ± 0.02	1.1 ± 0.2	0.065 ± 0.010		21.9
	Ni−C	2.81 ± 0.03	5.5 ± 1.7	0.110 ± 0.030		
Acetone	Ni−C/N	1.92 ± 0.02	2.8 ± 0.3	0.067 ± 0.007	26.6	3.70−12.00
EXAFS in solution	Ni−Br	2.31 ± 0.02	1.1 ± 0.2	0.059 ± 0.009		21.9
	Ni−C	2.84 ± 0.03	3.9 ± 1.1	0.077 ± 0.023		
Collidine	Ni−C/N	1.90 ± 0.02	3.2 ± 0.3	0.095 ± 0.008	28.1	3.80−12.00
EXAFS in solution	Ni−Br	2.29 ± 0.02	0.8 ± 0.1	0.067 ± 0.010		22.9
	Ni−C	2.82 ± 0.03	4.6 ± 1.4	0.112 ± 0.030		
Pyridine	Ni−C/N	1.90 ± 0.02	3.8 ± 0.3	0.072 ± 0.007	28.0	3.80−15.00
EXAFS in solution	Ni−C	2.82 ± 0.03	5.0 ± 1.5	0.087 ± 0.026		21.9
Acetonitrile	Ni−N	2.06 ± 0.02	6.1 ± 0.6	0.077 ± 0.007	23.5	3.38−14.00
Solid product after 3 h reaction,	Ni−C	2.24 ± 0.03	2.7 ± 0.4	0.091 ± 0.014		23.6
EXAFS in the solid state	Ni−C	2.84 ± 0.03	3.5 ± 1.1	0.110 ± 0.033		
	Ni−Ni	3.05 ± 0.03	2.1 ± 0.6	0.099 ± 0.026		
Butyronitrile	Ni−N	2.08 ± 0.02	6.4 ± 0.7	0.063 ± 0.007	21.8	3.47−11.00
Solid product after 12 h reaction,						41.9
EXAFS in the solid state						
Benzonitrile	Ni−N	2.07 ± 0.02	6.3 ± 0.7	0.074 ± 0.007	24.5	3.47−11.00
Solid product after 12 h reaction,						44.0
EXAFS in the solid state						
Methanol	Ni−O	2.06 ± 0.02	6.4 ± 0.3	0.071 ± 0.007	20.7	3.30−12.90
Solid product after 48 h reaction,	Ni−C	2.95 ± 0.03	6.2 ± 1.5	0.071 ± 0.023		31.6
Solid state EXAFS	Ni−Ni	3.09 ± 0.03	3.5 ± 1.5	0.077 ± 0.023		
H_2O/acetone (1:1.23)	Ni−O	2.05 ± 0.02	6.4 ± 0.3	0.087 ± 0.007	23.8	3.56−12.49
solid product after 12 h reaction,	Ni−Ni	3.07 ± 0.03	1.9 ± 1.5	0.081 ± 0.023		33.9
EXAFS in the solid state						
Pure	Ni−C/N	1.93	3			
Single crystal XRD[17]	Ni−Br	2.30	1			
	Ni−C	2.85	5			
$C_{31}H_{52}C_{l4}N_4Ni_4O_{15}$	Ni−O	2.07	6			
Methanol	Ni−Ni	3.09	3			
Single crystal XRD[48]						
$[Ni(NCCH_3)_6][SbF_6]$	Ni−N	2.08	6			
Single crystal XRD[50]	Ni−C	2.23	2			
	Ni−C	2.46	4			
	Ni−Ni	2.92	4			

in Table 2. Comparison of the experimental EXAFS functions in Figure 4 (c and d) shows that the complex in pyridine solution is not identical to [(bpy)Ni(Mes)(py)]NO_3, but exhibits a very similar spectrum to $[(py)_3$Ni(Mes)]Br. In [(bpy)Ni(Mes)(py)] two different Ni−C_{Mes}/N and Ni−N distances for the first coordination sphere were observed at 1.93 Å (*N* = 3.1) and 2.11 Å (*N* = 1.4), possibly due to the rigidity of the bipyridine ligand, which endeavors to keep a chelate bite angle of 82−83°. In $[(py)_3$Ni(Mes)]Br the first coordination sphere was fitted, as well as the pyridine solution, with only one shell at 1.90 Å (*N* = 4.2). In $[(py)_2$Ni(Mes)Br] the Ni−C_{Mes}/*N* distance of 1.88 Å (*N* = 3.2) agrees with those found in $[(py)_3$Ni(Mes)]Br and the pyridine solution. The quite long Ni−Br−distance in $[(py)_2$Ni(Mes)Br] of 2.40 Å is a consequence of a *trans* orientation of the mesityl and the bromide ligand.

In agreement with the other spectroscopic results we conclude that, in pyridine, [(bpy)Ni(Mes)Br] undergoes a ligand exchange reaction in which the bromide and bipyridine ligands are replaced, but the geometry of the first coordination shell around the nickel atom remains square-planar. The stability of [(bpy)Ni(Mes)Br] in collidine is due to the bulky nature of both the collidine and mesityl ligands, which prevents associative substitution.

Table 2. Structural parameters of solid reference Ni^{II} complexes determined from Ni *K*- and Br *K*-edge EXAFS spectra; [absorber A, backscatterer Bs, A−Bs distance *r*, coordination number *N*, Debye-Waller factor σ with calculated deviation, shift of the energy threshold energy ΔE_0 and the fit-index *R* (AFAC = 0.8)]

	A−Bs	*r* [Å]	N	σ [Å]	ΔE_0 [eV]	*k*-range [$Å^{-1}$] fit-index
[(bpy)Ni(Mes)(py)]NO_3	Ni−C/N	1.93 ± 0.02	3.1 ± 0.3	0.074 ± 0.008	27.8	3.70−13.50
EXAFS in the solid state	Ni−N	2.11 ± 0.02	1.4 ± 0.2	0.063 ± 0.011		38.9
	Ni−C	2.86 ± 0.03	4.9 ± 2.0	0.110 ± 0.030		
[$(py)_2$Ni(Mes)Br]	Ni−C/N	1.88 ± 0.02	3.2 ± 0.3	0.075 ± 0.008	28.9	3.40−11.50
EXAFS in the solid state	Ni−Br	2.40 ± 0.02	1.0 ± 0.2	0.076 ± 0.011		26.1
	Ni−C	2.80 ± 0.03	6.4 ± 2.0	0.099 ± 0.030		
	Br−Ni	2.39 ± 0.02	1.1 ± 0.1	0.081 ± 0.007	21.0	3.90−12.50
						32.3
[$(py)_3$Ni(Mes)]Br	Ni−C/N	1.90 ± 0.02	4.2 ± 0.3	0.072 ± 0.008	28.0	3.70−15.10
EXAFS in the solid state	Ni−C	2.82 ± 0.03	5.0 ± 1.5	0.087 ± 0.011		31.3
[(bpy)Ni(Mes)(MeO)]	Ni−C/N/O	1.89 ± 0.02	3.9 ± 0.3	0.070 ± 0.007	25.8	3.70−12.00
EXAFS in the solid state	Ni−C	2.82 ± 0.03	4.1 ± 1.2	0.080 ± 0.024		37.6
[$(phen)_2NiBr_2$][a]	Ni−N	2.05 ± 0.02	4.5 ± 0.5	0.068 ± 0.007	27.7	4.10−12.50
EXAFS in the solid state	Ni−Br	2.50 ± 0.03	2.1 ± 0.5	0.104 ± 0.011		43.4
	Br−Ni	2.49 ± 0.03	0.9 ± 0.1	0.063 ± 0.007	28.6	4.10−11.30
						56.6
$Ni(OH)_2$	Ni−O	2.07 ± 0.02	6.0	0.068 ± 0.007	23.5	3.70−13.50
EXAFS in the solid state	Ni−Ni	3.12 ± 0.03	6.0	0.077 ± 0.023		37.2
$Ni(OH)_2$	Ni−O	2.12	6			
powder ND[49]	Ni−Ni	3.13	6			

[a] phen = 1,10-phenanthroline.

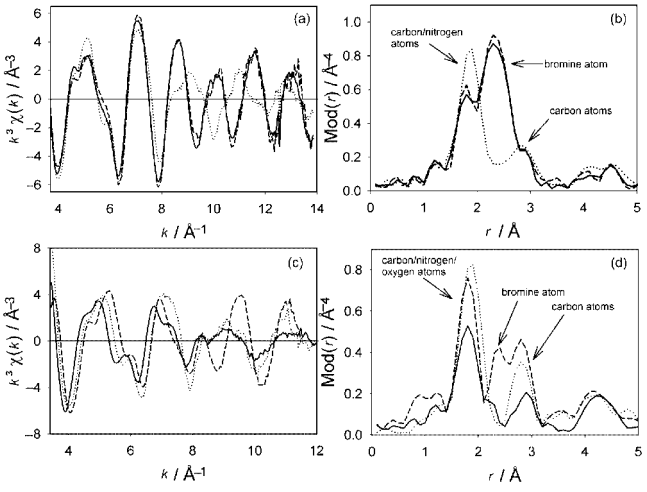

Figure 4. Comparison of the experimental $k^3\ \chi(k)$ functions (a) and their Fourier transforms (b) of solid [(bpy)Ni(Mes)Br] (solid line) with its solutions in THF (dashed line) or pyridine (dotted line) (Ni *K*-edge); comparison of the experimental $k^3\ \chi(k)$ functions (c) and their Fourier transforms (d) of solid [(bpy)Ni(Mes)(py)]NO_3 (solid line), [$(py)_3$Ni(Mes)]Br (dotted line) with solid [$(py)_2$Ni-(Mes)Br] (dashed line) (Ni *K*-edge)

From the XANES spectra it is evident that, in nitriles, alcohols and mixtures of acetone and water, the complex changes from square-planar to octahedral. The solubility of the complex in nitriles and alcohols is sufficient to carry out XANES experiments in transmission mode. For EXAFS investigations, however, the quality of the spectra obtained in solution was not satisfactory. Therefore the reaction mixtures were concentrated to dryness and the EXAFS measurements performed on the solid reaction products. In all the above-mentioned cases an octahedral coordination of the Ni atom was confirmed by EXAFS.

The distance of the first coordination shell from the metal ion is in all cases higher than in the square-planar complexes and consistent with the $Ni-N_{Phen}$ distance of 2.05 Å found in the octahedral reference compound [(1,10-phenanthroline)$_2$NiBr$_2$] (see Table 2).

Figure 5 shows the EXAFS spectra and the Fourier transforms of the products of the reaction of **1** in methanol after 2 or 48 h reaction, respectively, measured at the Ni *K*-edge [Figure 5 (a and b)] and Br *K*-edge [Figure 5 (c and d)]. The bromine FT-EXAFS spectrum of the product after 2 h of reaction in methanol [Figure 5 (b)] still shows a significant, but weak, contribution of nickel backscatterers to the signal. The fit of the EXAFS function led to a coordination number of 0.3, thus revealing that the reaction product after 2 h is still a mixture of bromide-containing square-planar and octahedral species. The EXAFS spectrum at the Ni *K*-edge of the product after 48 h reaction in methanol [Figure 5 (a)] was fitted with three coordination shells. The first coordination shell was fitted with oxygen backscatterers at 2.06 Å and proved the sixfold coordination of the nickel atom ($N = 6.5 \pm 0.6$). The very intense signal at about 3 Å in the FT EXAFS spectrum [Figure 5 (b)] is due to C backscatterers at 2.95 Å ($N = 6.2$) and Ni backscatterers at 3.09 Å ($N = 3.5$). These structural parameters fit the reported crystal structure of a (methanol)Ni^{II} complex.[48] In addition to the EXAFS investigations, the ^{1}H NMR spectrum of the [D_6]acetone extract of the prod-

uct obtained after 48 h showed the presence of uncoordinated bipyridine and mesitylene. Thus, in methanol, complete ligand exchange of all ligands (bromide, bipyridine and mesityl) against methanol molecules has taken place. That the Ni atoms in the methanolic product are only surrounded by oxygen atoms can be shown by comparison of the EXAFS spectra of solid $Ni(OH)_2$ with the product. In $Ni(OH)_2$ the Ni atoms are surrounded by six oxygen atoms at a similar distance (2.07 Å), as in the methanolic product. Furthermore, $Ni(OH)_2$ reveals an Ni−Ni distance (3.12 Å) that is almost identical with the one found in the methanolic product. The EXAFS spectrum and the FT of $Ni(OH)_2$ have been added to Figure 5 (a and b). The intensity of the first signal in the FT of both compounds is almost identical, which can be correlated with the same number and type of backscatterers in these compounds. The signal of the Ni backscatterers at 3.12 Å in $Ni(OH)_2$ is higher due to the higher coordination number of 6 in $Ni(OH)_2$.[49]

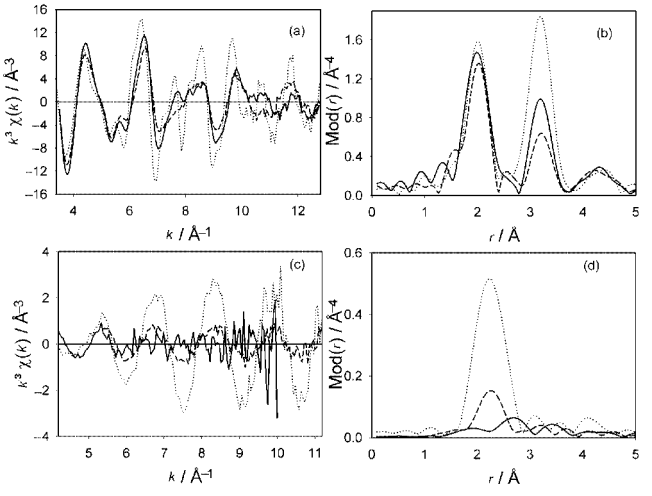

Figure 5. Comparison of the experimental k^3 $\chi(k)$ functions (a) and their Fourier transforms (b) of the isolated solid product of [(bpy)Ni(Mes)Br] in methanol after 2 h reaction (dashed line) and after 48 h reaction (solid line) with solid $Ni(OH)_2$ (dotted line) (Ni *K*-edge); comparison of the experimental k^3 $\chi(k)$ functions (c) and their Fourier transforms (d) of solid [(bpy)Ni(Mes)Br] (dotted line) with the isolated solid products of [(bpy)Ni(Mes)Br] in methanol after 2 h reaction (dashed line) and after 48 h reaction (solid line) (Br *K*-edge)

In the EXAFS function of the solid product of [(bpy)Ni(Mes)Br] in acetonitrile after 3 h reaction [Figure 6 (a)] the contribution of Ni backscatterers was similar to that of the product of the methanol solution. The structural parameters determined from the Ni *K*-edge EXAFS spectrum agree quite well to the acetonitrile complex $[Ni(CH_3CN)_6]SbF_6$,[50] in which the acetonitrile molecules have a bridging position between the Ni atoms. ^1H NMR experiments on the acetonitrile product have proved the splitting of the bpy and the mesityl ligand (as mesitylene), the latter seems to be a pre-requisite to the formation of octahedral species.

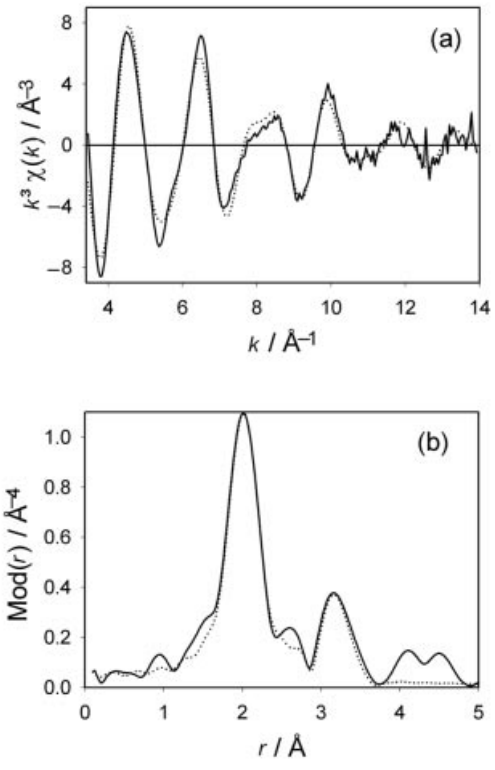

Figure 6. Experimental (solid line) and calculated (dotted line) k^3 $\chi(k)$ function (a) and their Fourier transform (b) of the isolated solid product of [(bpy)Ni(Mes)Br] acetonitrile after 3 h reaction (Ni *K*-edge)

Structural Studies on the [(*i*Pr-DAB)Ni(Mes)Br] System

Crystal Structure

In the crystal structure of [(*i*Pr-DAB)Ni(Mes)Br] (Figure 2) no intermolecular interactions other than van der Waals were found. The structure was solved with a disorder on one of the two isopropyl substituents. The two positions were found to be occupied in a 60:40% ratio. However, this has no impact on the square-planar coordination sphere of the nickel atom. Deviation towards the tetrahedron is only 9.3° and the angle C(11)−Ni(1)−N(2) deviates by 6.6° from the ideal 180°, thus resembling the less distorted molecule 1 of [(bpy)Ni(Mes)Br]·THF. The *trans* influence has a marked effect on the Ni−N bond lengths as Ni−N *trans* to the strong donor mesityl is about 100 pm longer than *trans* to Br. As expected, to reduce the inter-ligand interactions the isopropyl substituents point away from the coordination sphere.[51−53] Nevertheless, they might also shield the nickel center, along with the methyl substituents of the mesityl ligand,[17] as the distances of the two groups from the Ni atom are similar, ca. 3.5 Å and ca. 3.1 Å, respectively.

XANES Investigations

In Figure 3 (d) the XANES spectra of solid [(*i*Pr-DAB)-Ni(Mes)Br] and its solution in acetonitrile in dependence

of time are shown. The spectrum of the solid complex shows the typical two pre-peaks for square-planar Ni^{II} complexes. The acetonitrile solution after 30 min reaction also shows these two pre-peaks, which means that most of the Ni atoms have retained their square-planar geometry. After 120 min, the signal of the $1s \rightarrow 4p_z$ transition is significantly weaker, strongly indicating a change from square-planar to octahedral for the Ni atoms. After 330 min, the signal of the $1s \rightarrow 4p_z$ transition has vanished. Obviously, the geometry change was completed within 330 min, which is in good agreement with the rate constants determined by UV/Vis in the acetonitrile solution of [(bpy)Ni(Mes)Br].

EXAFS Investigations

The structural parameters of the [(*i*Pr-DAB)Ni(Mes)Br] system determined from the Ni *K*-edge and Br *K*-edge are summarized in Table 3. The obtained structural data of the pure, solid complex are in good agreement with those found from the single-crystal analysis. The experimental and calculated EXAFS functions and the FT (Ni *K*-edge) of the pure, solid complex can be seen in Figure 7 (a and b). To examine if [(*i*Pr-DAB)Ni(Mes)Br] shows a similar ligand exchange behavior to [(bpy)Ni(Mes)Br], a solution of the complex in acetonitrile was monitored by EXAFS spectroscopy. Because of the low solubility of the complex in acetonitrile the spectra were of low quality. Therefore the EXAFS functions were fitted with only one coordination shell, in the *k*-range of 2.8−8 $Å^{-1}$ [Figure 7 (c)], and showed that the coordination number of the first coordination shell increased from 3.1 nitrogen backscatterers after 30 min to 6.0 nitrogen backscatterers after 330 min. The determined average distance of 2.13 Å for the first coordination shell after 330 min is 0.07 Å higher than in the solid product of [(bpy)Ni(Mes)Br] in acetonitrile due to a higher mobility of the coordinated solvent molecules in the liquid state. From these experiments there is no evidence of an additional shielding of the nickel atom by the *i*Pr-DAB ligand compared to bpy.

Structural Studies on the $[(PPh_3)_2Ni(Mes)Br]$ System

Crystal Structure

As with the two diimine complexes the crystal structure of $[(PPh_3)_2Ni(Mes)Br]$ (Figure 2) reveals no significant intermolecular interaction. The coordination plane is nearly perfect, with only the Br ligand being slightly bent (by 3.8°) so that the Br−Ni−C1 angle is 176.2°. Concurrently, the angle P(1)−Ni−P(2) of 183.95° is larger than the ideal 180°. The mesityl ligand is oriented perfectly orthogonal to the coordination plane in contrast to the diimine complexes where tilt angles around 70° are found for the mesityl ligand. The molecular structure is thus similar to that of the related molecule $[(PMe_3)_2Ni(Ph)Br]$.[54] The Ni−P distances [2.214(2) Å and 2.202(2) Å] and the Ni−C(1) distance

Table 3. Structural parameters of solid [(*i*Pr-DAB)Ni(Mes)Br] and its solution in acetonitrile as determined from Ni *K*- and Br *K*-edge EXAFS spectra [absorber A, backscatterer Bs, A−Bs distance *r*, coordination number *N*, Debye-Waller factor σ with calculated deviation, shift of the energy threshold energy ΔE_0 and the fit-index *R* (AFAC = 0.8)]

	A−Bs	*r* [Å]	N	σ [Å]	ΔE_0 [eV]	*k*-range [$Å^{-1}$] fit-index
Pure	Ni−C/N	1.96 ± 0.02	3.1 ± 0.3	0.089 ± 0.008	29.9	3.70−11.50
Solid state EXAFS	Ni−Br	2.31 ± 0.02	0.8 ± 0.2	0.085 ± 0.011		28.3
	Ni−C	2.69 ± 0.03	4.2 ± 1.3	0.062 ± 0.030		
	Br−Ni	2.30 ± 0.02	0.9 ± 0.1	0.060 ± 0.007	17.4	3.90−12.00
						27.2
After 30 min reaction	Ni−N	2.11 ± 0.02	3.1 ± 0.3	0.097 ± 0.010	15.7	3.00−8.00
						28.3
After 60 min reaction	Ni−N	2.16 ± 0.02	3.6 ± 0.4	0.097 ± 0.010	13.5	3.00−8.00
						28.3
After 90 min reaction	Ni−N	2.15 ± 0.02	4.4 ± 0.4	0.097 ± 0.010	15.5	3.00−8.00
						28.3
After 150 min reaction	Ni−N	2.14 ± 0.02	4.9 ± 0.5	0.097 ± 0.010	16.7	3.00−8.00
						28.3
After 180 min reaction	Ni−N	2.14 ± 0.02	5.1 ± 0.5	0.097 ± 0.010	16.1	3.00−8.00
						28.3
After 210 min reaction	Ni−N	2.13 ± 0.02	5.3 ± 0.5	0.097 ± 0.010	17.7	3.00−8.00
						28.3
After 300 min reaction	Ni−N	2.14 ± 0.02	5.7 ± 0.6	0.097 ± 0.010	18.3	3.00−8.00
						28.3
After 330 min reaction	Ni−N	2.13 ± 0.02	6.0 ± 0.6	0.097 ± 0.010	18.7	3.00−8.00
						28.3
Pure	Ni−C/N	1.94	3			
Single-crystal XRD	Ni−Br	2.31	1			
	Ni−C	2.71	2			

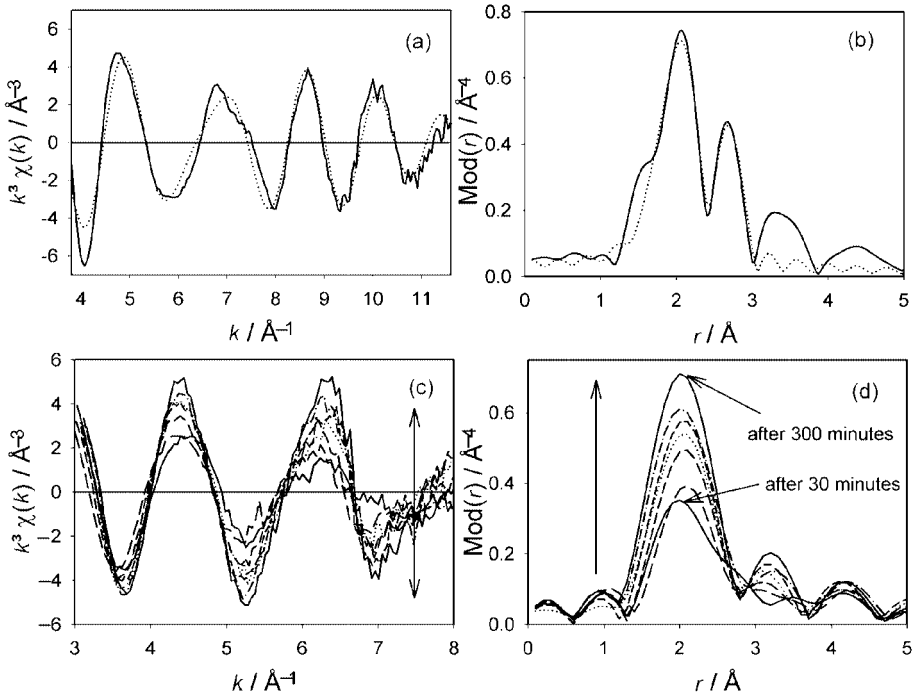

Figure 7. Comparison of the experimental $k^3\,\chi(k)$ functions (a) and their Fourier transforms (b) of [(*i*Pr-DAB)Ni(Mes)Br] in acetonitrile in dependence of time (after 30, 60, 120, 180, 240 and 300 min); experimental (solid line) and calculated (dotted line) $k^3\,\chi(k)$ functions (a) and their Fourier transforms (b) of solid [(*i*Pr-DAB)Ni(Mes)Br] (Ni *K*-edge)

[1.891(6) Å] in the latter are slightly shorter than can be explained by the bulkiness of the PPh_3 ligand. A marked difference lies in the orientation of the PR_3 ligands. The *trans*-oriented PPh_3 ligands show a nearly eclipsed conformation, whereas the PMe_3 ligands are staggered. Viewing the PPh_3 complex along an axis that parallels P(1)−Ni−P(2) one can see a graphite-like interaction of each one of the phenyl substituents with the nickel-bound mesityl ligand. This interaction might account for the eclipsed conformation, which probably leads to the steric repulsion of the phosphane ligands.

XANES Investigations

The XANES spectra of solid $[(PPh_3)_2Ni(Mes)Br]$ and its solid products formed by dissolving in acetonitrile, pyridine and collidine are shown in Figure 8. In all cases the 1s → $4p_z$ transition is clearly visible, identifying the complex and its solution products as square-planar. The 1s → 3d transition in all investigated complexes was very weak.

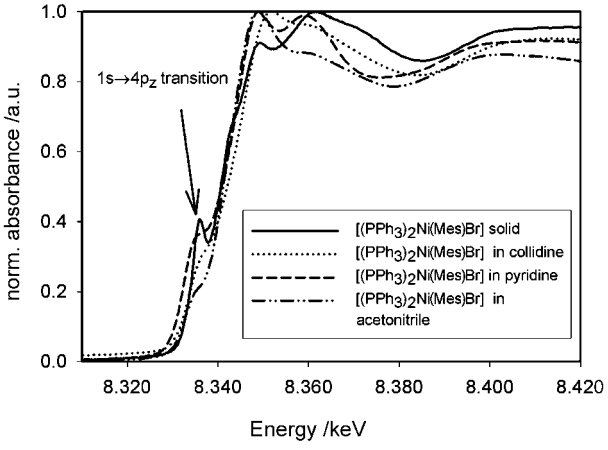

Figure 8. Comparison of the Ni *K*-edge XANES regions of solid $[(PPh_3)_2Ni(Mes)Br]$ with the solid products formed after 3 h in pyridine, collidine and acetonitrile

EXAFS Investigations

The solid $[(PPh_3)_2Ni(Mes)Br]$ was investigated at Ni *K*- and Br *K*-edge. The obtained structural parameters are summarized in Table 4. To fit the EXAFS function at the Ni *K*-edge three coordination shells were necessary. The determined values for the Ni−C_{Mes}, Ni−P and Ni−Br distances, as well as the coordination numbers of each shell, are in good agreement with the single-crystal experiment. EXAFS experiments on the solid products of $[(PPh_3)_2Ni(Mes)Br]$ in acetonitrile, pyridine and collidine after 3 h reaction are shown in Figure 9 (a and b). In all cases Br backscatterers did not contribute to the EXAFS functions. In contrast to the [(bpy)Ni(Mes)Br] and [(*i*Pr-DAB)Ni(Mes)Br] systems no geometrical change towards octahedral was observed in acetonitrile or THF solution. In the solid products of $[(PPh_3)_2Ni(Mes)Br]$ in acetonitrile or THF the coordination number of the first coordination shell is in total 4 (2 C/N + 2 P or 2 C/O + 2 P). The preservation of

Table 4. Structural parameters of solid $[(PPh_3)_2Ni(Mes)Br]$ and its reaction products in THF, acetonitrile, pyridine, or collidine determined from Ni *K*- and Br *K*-edge EXAFS spectra [absorber A, backscatterer Bs, A−Bs distance *r*, coordination number *N*, Debye-Waller factor σ with calculated deviation, shift of the energy threshold energy ΔE_0 and the fit-index *R* (AFAC = 0.8)]

	A−Bs	*r* [Å]	N	σ [Å]	ΔE_0 [eV]	*k*-range [Å^{-1}] fit-index
Pure	Ni−C	1.92 ± 0.02	1.1 ± 0.1	0.077 ± 0.007	25.0	3.50− 13.52
EXAFS in the solid state	Ni−P	2.23 ± 0.02	2.3 ± 0.3	0.081 ± 0.008		22.6
	Ni−Br	2.36 ± 0.02	1.1 ± 0.2	0.074 ± 0.011		
	Br−Ni	2.37 ± 0.02	1.0 ± 0.1	0.065 ± 0.007	16.0	3.90−15.00
						28.3
THF	Ni−C	1.91 ± 0.02	1.3 ± 0.1	0.081 ± 0.008	27.8	3.71−11.30
EXAFS in solution	Ni−O	2.07 ± 0.02	1.2 ± 0.2	0.055 ± 0.008		29.7
	Ni−P	2.21 ± 0.02	2.1 ± 0.2	0.089 ± 0.024		
Acetonitrile	Ni−C/N	1.98 ± 0.02	1.8 ± 0.2	0.089 ± 0.009	27.6	3.60−14.97
EXAFS in solution	Ni−P	2.25 ± 0.02	1.7 ± 0.3	0.063 ± 0.011		25.6
Pyridine	Ni−C/N	1.97 ± 0.02	3.1 ± 0.3	0.081 ± 0.008	24.0	3.50−11.00
EXAFS in the solid state	Ni−P	2.23 ± 0.02	0.9 ± 0.1	0.077 ± 0.011		23.3
	Ni−C	2.88 ± 0.03	6.0 ± 1.8	0.114 ± 0.034		
Collidine	Ni−C/N	1.91 ± 0.02	2.0 ± 0.2	0.050 ± 0.005	26.0	3.50−12.30
EXAFS in the solid state	Ni−P	2.22 ± 0.02	1.7 ± 0.3	0.081 ± 0.012		18.8
	Ni−C	2.80 ± 0.03	3.7 ± 1.0	0.089 ± 0.027		
Pure	Ni−C	1.91	1			
Single crystal XRD	Ni−P	2.24	2			
	Ni−Br	2.37	1			

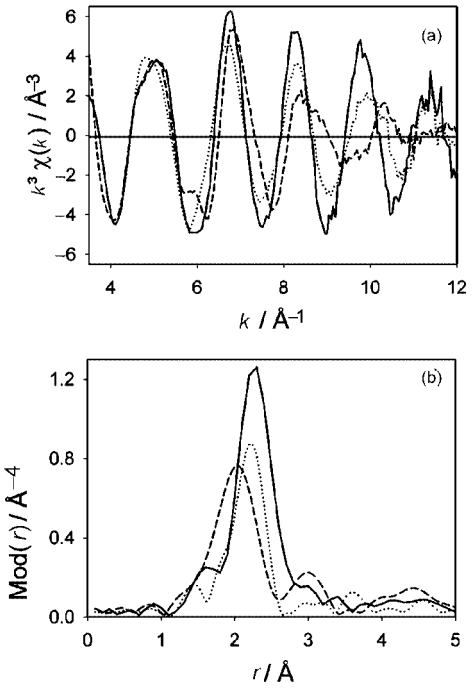

Figure 9. Comparison of the experimental $k^3\,\chi(k)$ functions (a) and their Fourier transforms (b) of solid $[(PPh_3)_2Ni(Mes)Br]$ (solid line) with the solid products of $[(PPh_3)_2Ni(Mes)Br]$ in acetonitrile (dotted line) or pyridine (dashed line)

the square-planar geometry can again be explained by the shielding mesityl ligand that prevents the formation of octahedral species. However, as to why in acetonitrile or THF solution the mesityl ligand is not split off as observed for the diimine complexes we can so far only speculate. Perhaps the steric hindrance of the bulky triphenylphosphane ligands prevents the hydrolysis reaction. Abstraction of the bromide ligand was also observed in the product obtained from the collidine solution. The $Ni-C_{Mes}/N_{Col}$ distance, however, is 0.07 Å shorter than in the acetonitrile product, since collidine is a better σ-donor ligand than acetonitrile.

It is noteworthy that [(bpy)Ni(Mes)Br] is stable in collidine solution, whereas for $[(PPh_3)_2Ni(Mes)Br]$ substitution of the bromide ligand was observed. Obviously, the bromide is a better leaving group in $[(PPh_3)_2Ni(Mes)Br]$ than in [(bpy)Ni(Mes)Br]. In pyridine solution the bromide ligand is replaced by the solvent as in the above-mentioned cases. Furthermore, substitution of one of the triphenylphosphane ligands was concluded from the increase in coordination number in the carbon/nitrogen shell from 1.2 in the pure complex to 3.1 in the pyridine solution and the decrease in the phosphorus coordination from 2.3 to 0.9.

Conclusion

A combined spectroscopic (multinuclear NMR, absorption) and structural investigation using XRD, XANES and EXAFS was successfully applied to monitor the ligand exchange behavior of three square-planar mesitylnickel(II) complexes, *cis*-[(diimine)Ni(Mes)Br] (diimine = 2,2′-bipyridine or *N*,*N*-diisopropyl-1,2-ethanediimine), and *trans*-$[(PPh_3)_2Ni(Mes)Br]$. The chosen system with bromide as the leaving ligand, the mesityl ligand as a strong donor and effective shielding group, as well as the *cis* (diimine ligands) and *trans* (PPh_3) variation of the complexes conformation has allowed us to draw some important conclusions.

The replacement of bromide is strongly accelerated when oriented *trans* to the strong donor ligand mesityl, which can be observed from the rapid splitting off of bromide from *trans*-[$(PPh_3)_2$Ni(Mes)Br] in weakly coordinating solvents such as acetone or THF in which the diimine complexes are stable. While further ligand exchange has never been reported for such complexes we have found that upon prolonged reaction times the diimine ligands or PPh_3 were also replaced by the solvent molecules, which is of great importance regarding the catalytic activity of such molecules. The rates of these reaction are smaller by orders of magnitude but this has to be viewed against the backdrop of long-term stability. In protic media such as alcohols the mesityl ligand is split off and, after the loss of this shielding group, octahedral nickel species are formed. Interestingly this is also valid for nitriles. The change in geometry from square-planar to octahedral can be readily monitored by XANES. Since the formation of such saturated octahedral species is concomitant with the breakdown of catalytic activity a successfully operating catalyst system has to contain a stable shielding unit. In the successfully applied systems by Brookhart and others this is provided by the diimine ligand, e.g. bulky R-DAB ligands with R = 2-6-dialkylated aryl substituents. However, we found that the diimine ligands can also be cleaved. Therefore, new long-term stable systems need to take account of the potential loss of the diimine ligand. In further studies we aim to develop catalytic systems with such long-term stability and apply them under real catalytic conditions.

Experimental Section

Preparations: All preparations were carried out under argon. The synthesis of the complexes [$(PPh_3)_2$Ni(Mes)Br] and [(bpy)Ni(Mes)Br] has been recently described.[17] All solvents were obtained from commercial sources and used as received. The alcohols and acetonitrile used were anhydrous. The other solvents were of spectroscopic grade.

Synthesis of [(*i*Pr-DAB)Ni(Mes)Br]: *i*Pr-DAB (250 mg, 1.78 mmol) was added to a vigorously stirred suspension of [$(PPh_3)_2$Ni(Mes)Br] (250 mg, 0.32 mmol) in 500 mL of *n*-pentane. After a few minutes, the yellow solid dissolved and at the same time a violet voluminous solid precipitated. After stirring for 4 h, the solid was filtered off, washed with pentane, recrystallized from CH_2Cl_2/*n*-heptane (1:8) and dried in vacuo to yield dark violet microcrystals. Yield: 112 mg (82%). $C_{17}H_{27}BrN_2Ni$ (398.03): calcd. C 57.07, H 6.59, N 31.60; found C 56.55, H 6.29, N 32.09. ^{1}H NMR ([D$_6$]acetone): δ = 8.55 (s, 1 H, H_{imine}), 8.43 (s, 1 H, H_{imine}), 6.42 (s, 2 H, *m*-H), 3.26 (m, 2 H, HC*i*Pr), 2.97 (s, 6 H, *o*-CH_3), 2.21 (s, 3 H, *p*-CH_3), 2.03 (d, 12 H, H_3C*i*Pr) ppm.

Synthesis of [(bpy)Ni(Mes)(OMe)]: Fine-cut sodium (100 mg, 4.35 mmol) was added to a mixture of 50 mL of THF and 10 mL of methanol. After all of the sodium had dissolved and reacted, [(bpy)Ni(Mes)Br] (400 mg, 0.97 mmol) was added to this solution. The red color of the starting material immediately turned to violet. After stirring for 3 h, the reaction solvents were evaporated to dryness and the residue extracted with 5 × 10 mL of CH_2Cl_2. The resultant Bordeaux colored solution was carefully filtered and then concentrated to dryness. Recrystallization from CH_2Cl_2/*n*-heptane (1:1) gave red-violet microcrystals. Yield: 290 mg (82%). $C_{20}H_{22}N_2NiO$ (365.12): calcd. C 65.79, H 6.07, N 7.67; found C 65.55, H 6.02, N 7.59. ^{1}H NMR ([D$_6$]acetone): δ = 9.0 [s (broad), 1 H, bpy-6], 8.31 (d, 1 H, bpy-3), 8.20 (d, 1 H, bpy-3′), 8.20 (dt, 1 H, bpy-4), 8.04 (dt, 1 H, bpy-4′), 7.71 (ddd, 1 H, bpy-5), 7.56 [s (broad), 1 H, bpy-6′), 7.21 (ddd, 1 H, bpy-5′), 6.57 (s, 2 H, *m*-H), 3.28 (s, 3 H, OCH_3), 3.07 (s, 6 H, *o*-CH_3), 2.20 (s, 3 H, *p*-CH_3) ppm. ^{13}C NMR ([D$_6$]acetone): δ = 156.4, 153.1, 151.5, 148.4, 148.3, 143.5, 139.6, 137.7, 127.3, 126.5, 132.8, 126.1, 122.4, 121.35, 69.1 (OCH_3), 25.8 (*o*-CH_3), 20.8 (*p*-CH_3) ppm.

Synthesis of [(bpy)Ni(Mes)(py)](NO$_3$): [(bpy)Ni(Mes)Br] (203 mg, 0.49 mmol) was dissolved in a mixture of 50 mL of acetone/acetonitrile (3:1) and thallium nitrate ($TlNO_3$) (133 mg, 0.5 mmol) and pyridine (40 mg, 0.5 mmol) were added to the red solution. $TlNO_3$ slowly dissolved while the reaction proceeded. After 5 h of stirring, the solution was orange-yellow and a greenish precipitate had formed that was carefully filtered off, and the filtrate was then concentrated to dryness. After washing the residue with 5 × 10 mL of diethyl ether, a bright yellow amorphous solid was obtained. Yield: 209 mg (90%). $C_{24}H_{24}N_4NiO_3$ (475.19): calcd. C 60.66, H 5.09, N 11.79; found C 60.36, H 5.01, N 11.68%. Due to the insolubility of the compound in common organic solvents no NMR spectra were obtained.

Synthesis of [(py)$_3$Ni(Mes)]Br: [(bpy)Ni(Mes)Br] (240 mg, 0.58 mmol) was dissolved in pyridine (30 mL) and stirred for 24 h. The volume was then reduced to 1/3 and *n*-octane (30 mL) added. The resultant yellow solution was stored at −30 °C overnight during which time a microcrystalline solid precipitated. After filtration, this solid was washed with *n*-pentane. Yield: 192 mg (67%). From the mother liquor further yellow material was isolated. However, this turned out to be a mixture of products. $C_{24}H_{26}BrN_3Ni$ (495.1): calcd. C 58.22, H 5.29, N 8.49; found C 58.18, H 5.21, N 8.44. ^{1}H NMR ([D$_6$]acetone): δ = 8.91 (d, 4 H, py-2,6), 8.18 (d, 2 H, py-2,6), 7.75 (t, 2 H, py-4), 7.46 (t, 1 H, py-4), 7.32 (dd, 4 H, py-3,5), 7.00 (dd, 2 H, py-3,5), 6.41 (d, 2 H, *m*-H), 3.45 (s, 6 H, *o*-CH_3), 2.21 (s, 3 H, *p*-CH_3) ppm. UV/Vis (pyridine): λ = 420 nm (ε = 320 M^{-1} cm^{-1}), 396 (sh, 320), 363 (1000), 323 (sh, 710).

Synthesis of *trans*-[(py)$_2$Ni(Mes)Br]: [$(PPh_3)_2$Ni(Mes)Br] (180 mg, 0.23 mmol) was dissolved in toluene (20 mL) and pyridine (80 mg, 1 mmol) was added to this red solution. After a few minutes, when the solution had turned yellow, the volume was reduced to 1/2. During storing of the solution at −20 °C overnight, yellow microcrystals had formed. Filtration and subsequent washing with *n*-pentane yielded a first crop (46 mg, 48%). The material that was further isolated from the mother liquor turned out to be a mixture including compounds of higher and lower degrees of substitution. $C_{14}H_{21}BrN_2Ni$ (416): calcd. C 54.86, H 5.09, N 6.73; found C 54.81, H 5.06, N 6.70. ^{1}H NMR ([D$_6$]acetone): δ = 8.96 (d, 4 H, py-2,6), 7.68 (t, 2 H, py-4), 7.20 (dd, 4 H, py-3,5), 6.33 (s, 2 H, *m*-H), 3.44 (s, 6 H, *o*-CH_3), 2.16 (s, 3 H, *p*-CH_3) ppm.

Synthesis of [(phen)$_2$NiBr$_2$]: [$NiBr_2$] (236 mg, 1.08 mmol) was added to DMF (10 mL) and dissolved on heating to 100 °C. Upon addition of 1,10-phenanthroline (390 mg, 2.16 mmol), the initially brownish solution turned green. On cooling to ambient temperature, a green solid precipitated that was collected by filtration, washed with diethyl ether and recrystallized from ethanol/diethyl ether (4:1). Yield: 562 mg (90%). $C_{24}H_{16}Br_2N_4Ni$ (578.93): calcd. C 49.79, H 2.79, N 9.68; found C 49.63, H 2.71, N 9.61. UV/Vis (MeCN): λ = 1055 nm (ε = 61 M^{-1} cm^{-1}), 631 nm (82), 326 (1040), 268 (26600), 226 (17860).

XANES and EXAFS Measurements: XANES and EXAFS measurements were performed at beamlines X1.1 (RÖMO II) and E4 at the Hamburger Synchrotronstrahlungslabor des Deutschen Elektronensynchrotrons (HASYLAB at DESY, Hamburg, Germany), at beamline 2−3 at the Stanford Synchrotron Radiation Laboratory (SSRL) at SLAC (Stanford, USA) and at beamline KMC-2 at the Berliner Elektronenspeicherring-Gesellschaft für Synchrotronstrahlung m.b.H. (BESSY II, Berlin, Germany). For measurements at the Ni *K*-edge (8332.8 eV) an Si(111) double crystal monochromator was used and at the Br *K*-edge (13474.0 eV) a Si(311) double crystal monochromator was used at SSRL and at DESY respectively. At BESSY a SiGe(220) double crystal (0.5% Ge/cm) monochromator was used for the nickel and the bromine *K*-edge. The synchrotron beam current was between 80 and 100 mA at HASYLAB (positron energy 4.45 GeV), between 100 and 250 mA at BESSY (electron energy 1.7 GeV) and between 80 and 100 mA at the SSRL (electron energy 1.7 GeV). The tilt of the second monochromator crystal was set to 40% harmonic rejection. The energy resolution was estimated to be about 0.7−1.0 eV for the Ni *K*-edge and 4.0 eV for the Br *K*-edge. Energy calibration was performed with the corresponding metal foils in the case of nickel, and with lead metal foil (Pb L_{III}-edge) in the case of bromine. The spectra were collected under ambient conditions at 25 °C in transmission mode with ion chambers. All ion chambers were filled with nitrogen for measurements at the Ni *K*-edge, and the second and third chamber filled with argon for measurements at the Br *K*-edge. The solid-state samples were embedded in a polyethylene matrix and pressed into pellets. Solutions of the complexes were measured in a specially designed transmission sample cell for liquids. The concentration of all samples was adjusted to yield an absorption jump of $\mu \approx 1.5$. Data evaluation started with removal of the background absorption from the experimental absorption spectrum by subtraction of a Victoreen-type polynomial. The background-subtracted spectrum was then convoluted with a series of increasingly broader Gauss functions and the common intersection point of the convoluted spectra was taken as energy E_0.[55,56] To determine the smooth part of the spectrum, corrected for pre-edge absorption, a piecewise polynomial was adjusted in such a way that the low-*R* components of the resulting Fourier transform were minimal. After division of the background subtracted spectrum by its smooth part, the photon energy was converted into photoelectron wave numbers *k*. The resulting EXAFS function was weighted with k^3. Data analysis in *k* space was performed according to the curved wave multiple scattering formalism of the program EXCURV92 with XALPHA phase- and amplitude-functions.[57] The mean free path of the scattered electrons was calculated from the imaginary part of the potential (VPI was set to −4.00) and an overall energy shift (ΔE_0) was assumed. The Amplitude Reduction Factor (AFAC) was set to a value of 0.8 in the case of both the Ni *K*-edge and Br *K*-edge.

NMR and UV/Vis Spectroscopy: ^{1}H, ^{13}C and ^{31}P NMR spectra were recorded with a Bruker AC 250 spectrometer. UV/Vis absorption spectra were recorded with a Bruins Instruments Omega 10 spectrometer. Kinetic data were fitted using a monoexponential decay assuming a first-order mechanism.

X-ray Crystallography: For compounds **1**−**3** data collection was performed at $T = 173(2)$ K with a Siemens P4 diffractometer using Mo-K_α radiation ($\lambda = 0.71073$ Å). The structures were solved by the Patterson method using the SHELXTL-PLUS package [58] and refinement was carried out with SHELXL-97 employing full-matrix least-squares methods on F^2 [59] with $F_o^2 \geq 3\sigma(F_o^2)$. Empirical absorption ($\psi$ scans) correction was performed for all three complexes. All non-hydrogen atoms were treated anisotropically, and hydrogen atoms were included by using appropriate riding models. CCDC-194378, -194379 and -194380 contain the supplementary crystallographic data for this paper. These data can be obtained free of charge at www.ccdc.cam.ac.uk/conts/retrieving.html [or from the Cambridge Crystallographic Data Centre, 12 Union Road, Cambridge CB2 1EZ, UK; Fax: (internat.) + 44-1223/336-033; E-mail: deposit@ccdc.cam.ac.uk].

Acknowledgments

We thank HASYLAB at DESY (Hamburg, Germany), the SSRL at SLAC (Stanford, USA) and BESSY (Berlin, Germany) for providing synchrotron radiation. The SSRL is operated by the U.S. Department of Energy, Office of Basic Energy Science. The authors would like to also thank Prof. Dr. Alexei Erko and Dr. Martin Fieber-Erdmann (BESSY GmbH, Berlin, Germany) for support during the beam times.

[1] S. Mecking, A. Held, F. M. Bauers, *Angew. Chem. Int. Ed.* **2002**, *41*, 544.
[2] S. D. Ittel, L. K. Johnson, M. Brookhart, *Chem. Rev.* **2000**, *100*, 1169.
[3] W. Keim, R. P. Schulz, *J. Mol. Catal.* **1994**, *92*, 21.
[4] W. Keim, A. Behr, B. Limbacker, C. Krüger, *Angew. Chem. Int. Ed. Engl.* **1983**, *22*, 503.
[5] K. Nomura, *Recent Res. Dev. Pure Appl. Chem.* **1998**, *2*, 473.
[6] C. S. Shultz, J. M. De Simone, M. Brookhart, *J. Am. Chem. Soc.* **2001**, *123*, 9172.
[7] C. S. Shultz, J. M. De Simone, M. Brookhart, *Organometallics* **2001**, *20*, 16.
[8] C. M. Killian, L. K. Johnson, M. Brookhart, *Organometallics* **1997**, *16*, 2005.
[9] S. Mecking, L. K. Johnson, L. Wang, M. Brookhart, *J. Am. Chem. Soc.* **1998**, *120*, 888.
[10] A. M. LaPointe, M. Brookhart, *Organometallics* **2001**, *17*, 1530.
[11] A. Michalak, T. Ziegler, *Organometallics* **2001**, *20*, 1521.
[12] S. Mecking, *Angew. Chem. Int. Ed.* **2001**, *40*, 534.
[13] A. Held, S. Mecking, *Chem. Eur. J.* **2000**, *6*, 4623.
[14] G. J. P. Britovsek, V. C. Gibson, D. F. Wass, *Angew. Chem. Int. Ed.* **1999**, *38*, 428.
[15] T. Yamamoto, M. Abla, *J. Organomet. Chem.* **1997**, *535*, 209.
[16] T. Yamamoto, S. Wakabayashi, K. Osakada, *J. Organomet. Chem.* **1992**, *428*, 223.
[17] A. Klein, *Z. Anorg. Allg. Chem.* **2001**, *627*, 645.
[18] A. Klein, M. P. Feth, H. Bertagnolli, S. Zális, manuscript in preparation.
[19] Y. H. Budnikova, J. Perichon, D. G. Yakhvarov, Y. M. Kargin, O. G. Sinyashin, *J. Organomet. Chem.* **2001**, *630*, 185.
[20] Y. H. Budnikova, O. E. Petrukhina, Y. M. Kargin, O. G. Sinyashin, *Zh. Obshch. Khim.* **1996**, *66*, 605.
[21] T. Yamamoto, A. Yamamoto, S. Ikeda, *J. Am. Chem. Soc.* **1971**, *93*, 3350.
[22] M. Martinez, G. Muller, *J. Chem. Soc., Dalton Trans.* **1989**, 1669.
[23] N. Kawata, K. Maruya, T. Mizoroki, A. Ozaki, *Bull. Chem. Soc. Jpn.* **1974**, *47*, 2003.
[24] H. Bock, H. Tom Dieck, *Angew. Chem.* **1966**, *78*, 549.
[25] D. J. Stufkens, *Coord. Chem. Rev.* **1990**, *104*, 39.
[26] R. W. Balk, T. L. Snoeck, D. J. Stufkens, A. Oskam, *Inorg. Chem.* **1980**, *19*, 3015.
[27] G. van Koten, K. Vrieze, *Adv. Organomet. Chem.* **1982**, *21*, 151.
[28] H. Bertagnolli, T. S. Ertel, *Angew. Chem. Int. Ed. Engl.* **1994**, *33*, 45.
[29] G. Kickelbick, U. Reinöhl, T. S. Ertel, H. Bertagnolli, K. Matyajaszewski, *The Copper Catalyst in Atom Transfer Radical Polymerizations: Structural Observations Controlled/Living Radical Polymerization* (Ed.: K. Matyaszewski), American Chemical Society, Washington, DC, **2000**, p. 211.

[30] E. Lindner, F. Auer, A. Baumann, P. Wegner, H. A. Mayer, H. Bertagnolli, U. Reinöhl, T. S. Ertel, A. Weber, *J. Mol. Catal. A* **2000**, *157*, 97.
[31] G. Kickelbick, U. Reinöhl, T. S. Ertel, A. Weber, H. Bertagnolli, K. Matyjaszewski, *Inorg. Chem.* **2001**, *40*, 6.
[32] F. Wong, F. W. Lytle, R. P. Messmer, D. H. Maylotte, *Phys. Rev.* **1984**, *B30*, 5596.
[33] A. Biaconi, *Springer Proc. Phys.* **1984**, *2*, 167.
[34] G. J. Colpas, M. J. Maroney, C. Bagyinka, M. Kumar, W. S. Willis, S. L. Suib, N. Baidya, P. K. Mascharak, *Inorg. Chem.* **1991**, *30*, 920.
[35] M. W. Renner, L. R. Furenlid, K. M. Barkigia, J. Fajer, *J. Phys. IV Fr.* **1997**, *7*, C2-661.
[36] A. Arcas, P. Royo, *Inorg. Chim. Acta* **1978**, *31*, 97.
[37] T. R. Miller, I. G. Dance, *J. Am. Chem. Soc.* **1973**, *95*, 6970.
[38] L. Sacconi, *Transit. Metal Chem.* **1968**, *4*, 199.
[39] D. Nicholls, "Nickel" in *Comprehensive Inorganic Chemsitry*, Pergamon Press, Oxford, **1973**, vol.3, p. 1109.
[40] R. H. Holm, M. J. O'Conner, *Inorg. Chem.* **1971**, *14*, 241.
[41] R. G. Hayter, F. S. Humiec, *Inorg. Chem.* **1965**, *4*, 1701.
[42] H. Weiss, F. Hampel, W. Donaubauer, M. A. Grundl, J. W. Bats, A. S. K. Hashmi, S. Schindler, *Organometallics* **2001**, *20*, 1713.
[43] P. T. Matsunaga, G. L. Hillhouse, *J. Am. Chem. Soc.* **1993**, *115*, 2075.
[44] M. Sato, Y. Fujii, T. Yamamura, S. Yano, *Bull. Chem. Soc. Jpn.* **1994**, *67*, 1954.
[45] R. Oritz, J. Borrás, L. Perelló, H. Jimenez, *Monatsh. Chem.* **1986**, *117*, 443.
[46] J. Mollin, Z. Pavelek, A. Schneiderova, J. Vicar, V. Simanek, J. Lasovsky, *Coll. Czech. Chem. Commmun.* **1983**, *48*, 2156.
[47] pK_a (methanol, 25 °C) = 15.32; pK_a (ethanol, H_2O, 90% molar content, 25 °C) = 16.29; pK_a (1-propanol, H_2O, 90% molar content, 25 °C) = 16.78; pK_a (2-propanol, H_2O, 90% molar content, 25 °C) = 17.97
[48] A. J. Blake, E. K. Brechin, A. Codron, R. O. Gould, C. M. Grant, S. Parsons, J. M. Rawson, R. E. P. Winpenny, *J. Chem. Soc., Chem. Commun.* **1983**, 1995.
[49] A. Szytula, A. Murasik, M. Balanda, *Phys. stat. sol. (b)* **1971**, *43*, 125.
[50] I. Leban, D. Gantar, B. Frlec, D. R. Russell, J. H. Holloway, *Acta Crystallogr., Sect. C* **1987**, *43*, 1888.
[51] H.-D. Hausen, K. Krogmann, *Z. Anorg. Allg. Chem.* **1972**, *389*, 247.
[52] S. Hasenzahl, H.-D. Hausen, W. Kaim, *Chem. Eur. J.* **1995**, *1*, 95.
[53] V. De Felice, P. Ganis, A. Vitagliano, G. Valle, *Inorg. Chim. Acta* **1988**, *144*, 57.
[54] H.-F. Klein, A. Bickelhaupt, M. Lemke, H. Sun, A. Brand, T. Jung, C. Röhr, U. Flörke, H. J. Haupt, *Organometallics* **1997**, *16*, 668.
[55] T. S. Ertel, H. Bertagnolli, S. Hückmann, U. Kolb, D. Peter, *Appl. Spectrosc.* **1992**, *46*, 690.
[56] M. Newville, P. Livins, Y. Yakoby, J. J. Rehr, E. A. Stern, *Phys. Rev. B* **1993**, *47*, 14126.
[57] S. J. Gurman, N. Binsted, I. Ross, *J. Phys. C* **1986**, *19*, 1845.
[58] G. M. Sheldrick, *SHELXTL-PLUS: An Integrated System for Solving, Refining and Displaying Crystal Structures from Diffraction Data*; Siemens Analytical X-ray Instruments Inc., Madison, WI, **1989**.
[59] G. M. Sheldrick, *SHELXL-97: A program for Crystal Structure Determination*; Universität Göttingen, Göttingen, **1997**.

Received July 11, 2002
[I02382]